EUROPEAN ORGANISATION FOR NUCLEAR RESEARCH
CERN – A&B DEPARTMENT

AB-Note-2007-004 ABP

Transfer Line Studies from LINAC4 to the PS Booster: "South Hall" Option

G. Bellodi, A. M. Lombardi

Abstract

Linac4 is a new normal conducting H^- linac, which is currently under study at CERN as upgrade to the present LHC injectors chain in view of intensifying the proton flux available for the CERN accelerator complex and eventually attain LHC ultimate luminosity goals. The new linac is designed to accelerate a 65 mA H^- ion beam from 3 MeV up to 160 MeV for charge-exchange injection into the CERN Proton Synchrotron Booster, thus overcoming the space charge limitations of the present injection mechanism at 50 MeV, which represent the main obstacle to obtaining higher beam brightness into the PS.
A new transfer line is also being planned to transport the beam from the end of Linac4 to the PSB and the present paper outlines one of the proposed layouts and gives the status of the beam dynamics studies for this solution.

Geneva, Switzerland
January 2007

Introduction

Linac4 is a new H^- linear accelerator presently studied at CERN. This machine consists of normal-conducting structures operating at 352.2 MHz and 704.4 MHz re-using the RF equipment from the decommissioned LEP collider. It is designed to replace the existing Linac2 and to inject the beam into the CERN PS Booster (PSB) at 160 MeV instead of the present 50 MeV injection energy to overcome the space-charge limitations. At the same time it is a front-end for the future high power 3.5 GeV superconducting linac (SPL) [1]. A more detailed description of the project can be found in the Technical Design Report [2]. A new transfer line will have to be built to transport the beam from the end of Linac4 to the PS Booster . As for the present Linac2 design at 50 MeV, the beam is completely debunched before injection (no limits on the phase width), but the energy spread needs to be constrained to guarantee reasonably low losses at RF capture in the Booster. The injection painting mechanism and the beam distribution in the four rings of the Booster also impose constraints on the transverse beam size, divergence and on the value of the dispersion function at the end of the line. The design of the transfer line has therefore been optimized in an attempt to satisfy at best all the beam dynamics requirements, under the obvious constraints imposed by the layout choice and while keeping to a minimum the number of beamline elements to contain costs.

Layout

At the time of writing three different sites are under consideration for the proposed construction of Linac4: the PS South Hall option (building 150), a Linac2 "extension" option (building 363) and finally a "greenfield" option in a tunnel to be newly excavated under the Mont Citron area.

The transfer line study outlined in this paper refers to the first of these scenarios, the others being discussed in a separate note [3]. For the case here considered, significant constraints on the choice of layout have been imposed by the necessity of integration in the complex of existing accelerator structures and also by the rationale of keeping Linac2 operational for the whole duration of Linac4 commissioning. The layout finally proposed after several attempts is shown in Figure 1, and a sketch of the line showing the positions of the different elements is provided in the Appendix A (Figure 10).

The line is bent soon after the end of Linac4 to go round the LEIR ring, it then enters the PS tunnel, crosses the LEIR injection/extraction line and Linac3 transfer line and finally joins the existing transfer line from Linac2 to the PSB just upstream of the BHZ30 dipole; the total length of the line up to the injection point in the Booster is 197.5m, of which 88m are along the old transfer line and 109.5m along the new part. This new part can be approximately divided in three straight sections joined by bendings: one short matching line at the exit of Linac4 (the last quadrupole of the Side Coupled Linac is used to match the beam into the transfer line) and two long doublet channels. The first long straight section passes close to the LEIR wall and then crosses the shielding wall of the PS with a long pipe without magnetic elements. The decision to move to a doublets structure from an originally chosen F0D0 structure for the beam focusing was motivated by the necessity to traverse the PS shielding wall with the minimum impact (i.e. without magnetic elements) to simplify the civil engineering involved (lower costs) and also for radiation protection issues (to minimize the flux of radiation from the PS). The second straight section passes close to the PS and then crosses the wall of the inflector area, traversing the Linac3 and LEIR transfer lines and finally joining the existing Linac2 line just upstream of the LT.BHZ30 dipole.

Transverse focusing is provided by 23 quadrupoles, which are 250 mm long and have a 70 mm aperture diameter. They can be coupled in pairs on a same power supply and the maximum gradient does not exceed 8 T/m (see Table1 for detailed magnet specifications, and Table 5 in the Appendix A for individual field settings).

Five dipole magnets are used for bending the line with a magnetic field B=1.0125 T, and angles of 17.275, 17.275, -10.55, 31 and 31 degrees respectively. From a manufacturing point of view, the bendings can be grouped in two different families, with the specifications summarised in Table 1.

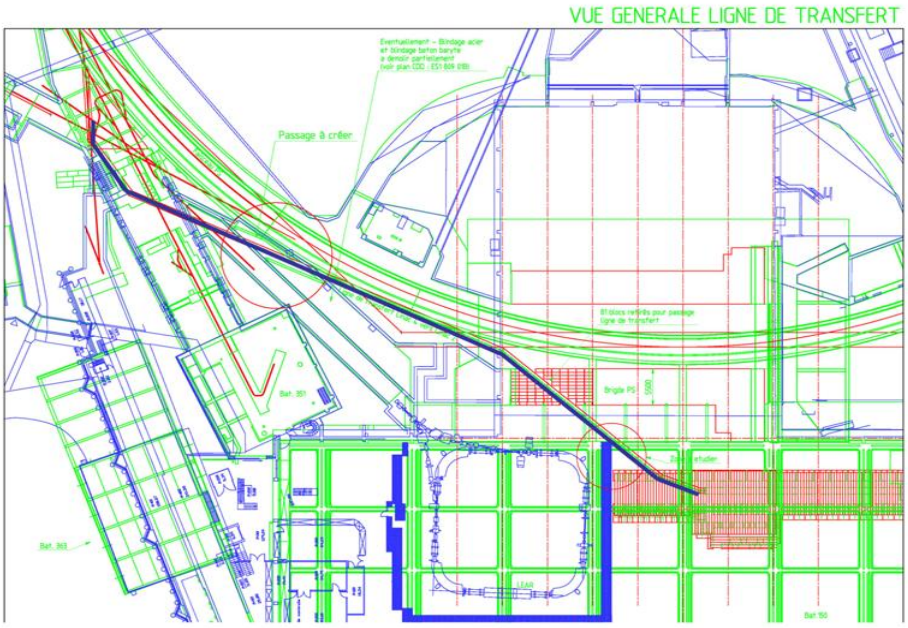

Figure 1: Layout of the Linac4 transfer line (South Hall option).

23 TL quadrupoles		
Magnet characteristics		
Gradient	8.0	T/m
Aperture radius	35.0	mm
Iron length	250.0	mm
Effective length	278.0	mm
∫Gdl	2.22	Tm/m
Dimensions		
Total magnet length	277	mm
Total magnet width	270	mm
Total magnet height	270	mm
Total magnet weight	97.1	kg
Electrical parameters		
Max. Current	200	A
Duty cycle	5.0	%
RMS current	10.1	A
Magnet resistance at 20 C	89.3	mOhm
Inductance	3.6	mH
Max. Voltage	741	V
Max. Dissipated power (pulsed)	9.1	W

Type A bending magnets		
Magnet characteristics		
Magnet field	1.0	T
Gap height	70.0	mm
Gap width	150.	mm
Iron length	600.	mm
Effective length	677.	mm
∫Bdl	0.677	Tm
Deflection angle	357	mrad
Dimensions		
Total magnet weight	805	kg
Total magnet length	788	mm
Total magnet width	530	mm
Total magnet height	378	mm
Electrical parameters		
Current	1000	A
Magnet resistance (hot)	24.3	mOhm
Max. Dissipated power per magnet (pulsed)	2.1	kW
Inductance	8.2	mH
Cooling parameters		
Pressure drop	1.0	bar
Temperature rise	11.0	K
Total cooling flow	2.7	l/min

Type B bending magnets		
Magnet characteristics		
Magnet field	1.0	T
Gap height	70.0	Mm
Gap width	150.0	Mm
Iron length	1000.	Mm
Effective length	1077.	Mm
∫Bdl	1.077	Tm
Deflection angle	573	mrad
Dimensions		
Total magnet weight	1329	kg
Total magnet length	1188	mm
Total magnet width	530	mm
Total magnet height	378	mm
Electrical parameters		
Current	1000	A
Magnet resistance (hot)	35.7	mOhm
Max. Dissipated power per magnet (pulsed)	4.0	kW
Inductance	13.1	mH
Cooling parameters		
Pressure drop	3.0	bar
Temperature rise	14.0	K
Total cooling flow	4.1	l/min

Table 1 Transfer line new magnet specifications [4]

An RF system is needed to rotate the beam in the longitudinal phase space from the initial upright position (with large energy spread and small phase width) to the final horizontal position, corresponding to a beam almost completely debunched and a minimum energy spread matched to the acceptance of the PS Booster. Studies have shown that two 352 MHz 5-cell cavities with voltages of 0.5 MV and 0.7 MV respectively will be sufficient to control the energy spread of the beam during transport and at injection, with no strong sensitivity on possible beam current variations. The position of the first cavity is chosen as a balance between letting the growth in energy spread of the beam under space charge effects reach saturation and avoiding the introduction of RF non-linearities that occur once the beam phase width is larger than the linear region of the RF slope ($\Delta\phi<50^o$). In the present scheme, a location approximately 20 m downstream of the Linac4 exit has been chosen. In order to allow for a better matching of the energy spread of the beam to the acceptance requirements of the PSB, a second cavity has been foreseen about 48m downstream, with an applied voltage of 0.7 MV(and the possibility of a third one is currently being explored as explained in a later paragraph). The required aperture radius for the two cavities (7 times rms beam size) is 35 mm and the overall length slightly over 1.1m (see Fig.2).

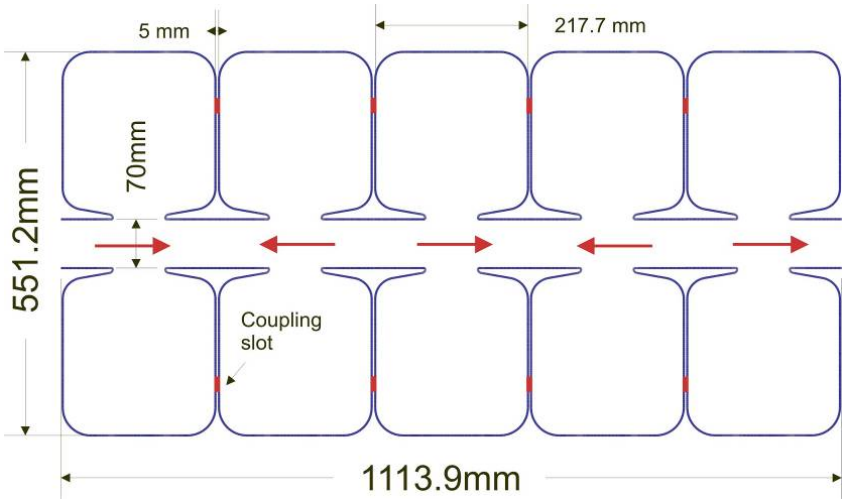

Figure 2 Layout of debunching cavity [5]

The line section passing inside the PS tunnel comes close to the PS magnets, with the point of closest approach being at only 2.5m from the PS beam trajectory. In order to avoid interferences from the PS magnetic fields, magnetic screening of the Linac4 beam pipe is foreseen. A study based on a 2D simulation of the CERN PS dipoles magnetic fields and analytical calculations [6] has shown that a 0.1mm thick layer of shielding material should be sufficient to reduce by a factor of 10 any induced stray fields, to the level of the earth's magnetic field. The attenuation factor has been approximated as $A \approx \mu_r t / 2b$, where b=100mm is the beampipe diameter, t the shielding thickness and μ_r=15000 is the magnetic permeability.

Another problem that was looked into is the probability of H- stripping in the dipoles, due to the effect of the electric field seen by a moving particle when passing through the magnetic field of a bending magnet. The average lifetime of the H^- ions has been calculated according to:

$$\tau(B) = \frac{7.96 \cdot 10^{-6}}{c\beta\gamma B} \exp\left(\frac{4.256 \cdot 10^{9}}{c\beta\gamma B}\right) \text{[7]}$$

and the stripping probability as $P = 1 - \exp(-t/\tau)$, where t is the time it takes the particle to traverse the dipole. For B=1T, ρ=2m, θ=30 deg and $\beta\gamma$=0.614 this has been found to be less than 0.002%.

For the part of the transfer line after the last bending (where it joins the existing Linac2 line) and up to the Booster injection, it is planned to keep all the existing equipment (quadrupoles and steerers); only the transverse focusing will have to be readjusted to the different beam energy (and therefore new power supplies will probably be required), in order to meet the new beam size and orientation requirements for matching into the PSB transverse acceptance. Table 2 lists for comparison the current and new settings of the magnets to be re-used along the LT/LTB/BI lines.

Quad name	Present settings@50MeV [T/m]	New settings@160MeV [T/m]	Max field [T/m]
LT.QFW70	0.65	-0.47	1.6
LT.QDN75	-0.65	0.37	4.19
LTB.QFN10	1.48	-0.34	4.19
LTB.QDN20	-0.79	-1.21	4.19
LTB.QFW30	0.45	1.27	1.6
LTB.QDW40	-0.66	-1.06	1.6
LTB.QFW50	0.74	1.02	1.6
LTB.QDW60	-0.72	-1.10	1.6
BI.Q10	1.18	1.23	1.7
BI.Q20	-1.38	-1.29	1.7
BI.Q30	0.75	1.05	1.7
BI.Q40	-1.02	-0.69	1.7
BI.Q50	1.29	-1.96	7.5
BI.Q60	-1.41	1.98	7.5

Table 2 Present and new settings for the equipment in the existing part of the transfer line.

Beam dynamics

Several stages were followed in the design of the transfer line as described in this note, each one informed by the need to comply with several constraints of either structural nature or related to beam dynamics. Space availability in the South Hall (or lack thereof) has imposed the segmented geometry of the line, with three straight sections (6, 35 and 57m long respectively) joined by bendings before the connection to the existing LT line. An effort was also made to avoid the presence of any magnetic elements in the passages to be opened through separation or shielding walls, in order to reduce both the costs involved in the civil engineering process and the flux of radiation from one area to adjacent ones. This particular choice led to the adoption of a doublets scheme for the transverse focusing instead of a F0D0 structure (owing to the necessity to accommodate longer drifts in between quadrupoles) and also placed constraints on the location of the debuncher cavities.

From the beam dynamics point of view the main guidelines followed have been minimising the emittance increase and losses, keeping an aperture radius to RMS beam size ratio of at least 5, and matching the beam parameters at the end of the line to the PSB acceptance requirements.

In the longitudinal plane the maximum bucket height is given by:

$$\Delta \hat{W}_{\max} = \pm 2\left[\frac{qmc^3\beta_s^3\gamma_s^3 E_0 T(\varphi_s\cos\varphi_s - \sin\varphi_s)}{\omega}\right]^{1/2} = \pm 2\left[\frac{qmc^2\gamma_s^3\beta_s^2\beta\lambda E_0 T}{2\pi}\right]^{1/2}\Bigg|_{\varphi_s=-90}$$

which yields $\Delta W_{max}\approx 200$ keV for $f\sim 1$ MHz, $E=163$ MeV and for a PSB cavities voltage $\beta\lambda E_0 T=0.6$ kV [8], and therefore sets an upper limit on the 90% emittance value of the final energy spread of approximately 100 keV.

In the transverse plane there are preliminary indications [9] that the beam at the injection point should have small betatron amplitudes in both the horizontal and vertical planes (~5-10m) and $\alpha_x\approx 0$; the dispersion function D_x should also be lower than 1.4m, which is the nominal dispersion value in the Booster ring.

The most critical part from the beam dynamics point of view is at the beginning of the line, just after the SCL, where the beam has a large energy spread, and it is very compressed in phase. This in combination with the presence of dispersive elements and space charge effects at 65mA beam current, leads to a complex scenario, that is difficult to handle without allowing for some emittance growth.

A first study of the line was carried out in the longitudinal plane: here a choice was made to use debuncher cavities at 352.2 MHz (half the SCL frequency) because of ease of design and ready availability of some equipment at CERN. The location and number of the cavities were decided after studying the longitudinal beam debunching under space charge forces (while focusing it transversely through series of doublets): these are very strong in the first few metres of the line, as can be seen in Figure 3, causing a rapid blowup

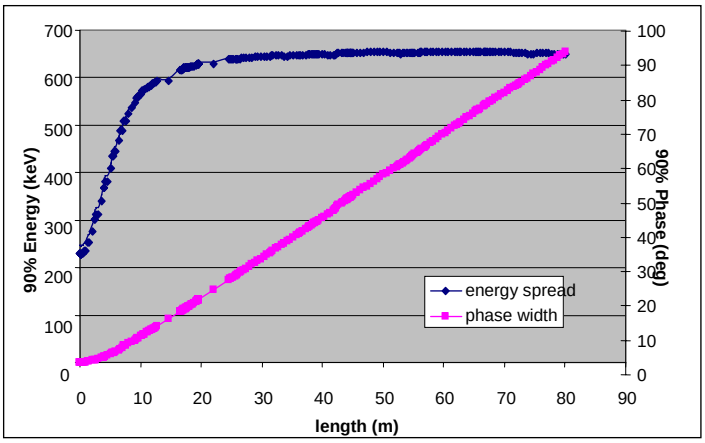

Figure 3 Evolution of the beam energy spread and phase width under space charge forces (90% emittance values).

in the energy spread of the beam. Bearing in mind all the structural constraints, the first cavity has been positioned at a point where the space charge forces have already reached some saturation, but not so far into the line as to introduce RF non-linearities related to a large beam phase width. A location some 19m downstream from the Linac4 exit was chosen, and a second cavity added at a distance of ~50m from the first in order to have an extra phase rotation for matching to $\Delta W<200$ keV and $\alpha_z \approx 0$ at injection into the PS Booster.

In the transverse plane a focusing scheme based on doublets has been adopted, for the necessity at times to leave up to 12-13 metres in between quadrupoles.

As mentioned earlier, the most problematic part to study was the ~35 degrees bend immediately after the exit from the SCL to go around the LEIR ring. An initial approach examined the possibility of using a locally achromatic system to control the emittance growth induced by the rapid increase in the energy spread of the beam in presence of dispersive elements. For this reason the bend joining the initial matching section with the first doublet channel was split into two identical dipoles with a triplet in between in order to match the dispersion function and its derivative to zero by tuning two of the quadrupoles. But due to the non-constant energy spread, even this solution could not prevent some residual emittance growth in the horizontal plane (~10%, as can be seen in Figure 4), that could only be reduced by shortening the overall length of the achromat (and therefore risking to put too much strain on the quadrupoles in the limits of the specifications given in Table 1).

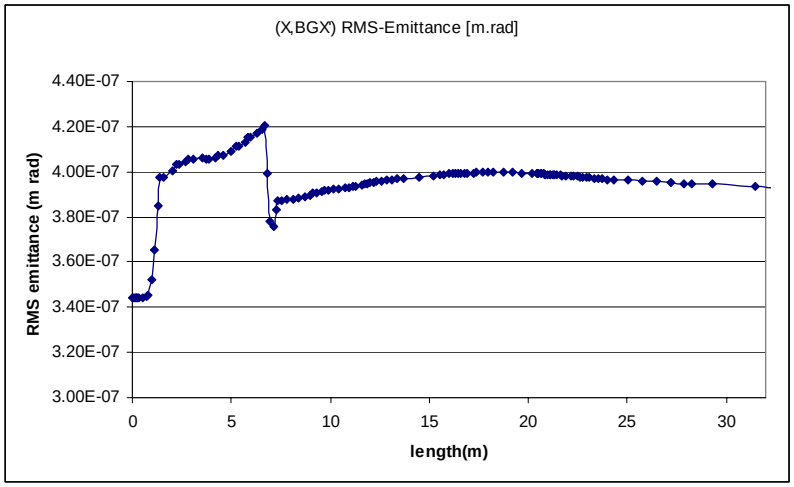

Figure 4 Horizontal emittance growth in the first part of the line (achromatic solution).

A more empirical approach was subsequently adopted, with an exploration of the phase space of the quadrupole gradients in the triplet of the achromat, to find the settings that minimize the initial growth in transverse emittance (to approximately 5%), regardless of the dispersion values.
For the same reasons, some consideration was also given to try and limit the longitudinal energy spread of the beam in the 'uncompensated' dipoles, as is the case for the double bend that directs the beam onto the old transfer line from Linac2 to the PSB, just upstream of the LT.BHZ30 dipole. From this point onwards, all existing equipment has been kept, just re-adjusting the strength of the magnets to the increased beam energy.
Injection into the Booster is via a charge-exchange mechanism with transverse and longitudinal painting, as described in [8]. At the end of the transfer line the beam is distributed to the four rings of the PSB via a sequence of a vertical bending magnet, a system of five pulsed magnets (distributor), a pre-deflector magnet and 3 septum magnets. The distributor and the septum have quite small apertures (25mm and 15mm respectively in the horizontal and vertical plane), making this area the acceptance bottleneck of the entire transfer line. A careful tuning of the quadrupoles has therefore to be implemented to keep a minimum aperture of at least 5 RMS (in terms of beam size) and also to give the beam an offset of 5.2mm at the distributor entrance, as prescribed by the injection scheme. It is also envisaged to connect the last quadrupoles of the line before the injection area to independent power supplies on a one-to-one scheme, in order to keep full tuning possibilities.
The beam dynamics design has been carried out using the program Trace3D, followed by more accurate fine tuning multi-particle simulations with the code PATH. At 160 MeV the beam (Fig.5) presents some halo, which is very well transmitted throughout the machine, and has an excessive energy spread that must be reduced to match the acceptance of the PS Booster.

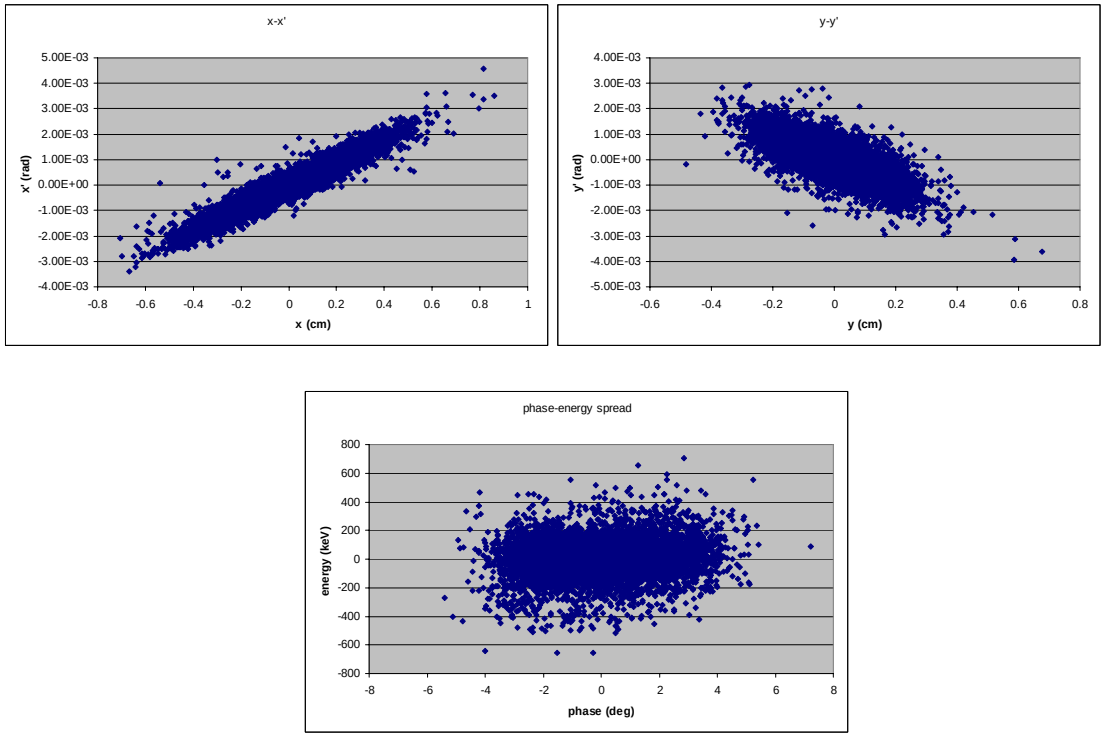

Figure 5 Beam phase space before last SCL quadrupole (at f=352.2 MHz).

Beam dynamics simulations were carried out using either an end-to-end distribution obtained from tracking the beam from the RFQ input to the end of the SCL (see phase space plots in Figure5) or an internally generated uniform distribution of 50k particles with the same emittances and Twiss parameters as the end-to-end one, as summarized in Table3.

	α	β	ε RMS
x	-3.23	7.50 m/rad	0.344 mm mrad
y	1.13	2.62 m/rad	0.344 mm mrad
z	-0.12	14.29 deg/MeV	0.189 deg MeV
Energy	163.05 MeV		
Current	65 mA		
Frequency	352.2 MHz		

Table 3 Input beam parameters

The beam has been transported along the ~200 m of the transfer line with no losses (or very negligible, less than 0.05%).
The evolution of the RMS beam envelopes is shown in Fig.6: beam sizes are mostly contained within 5mm and present a fairly regular behaviour along the line. The RMS emittance growth in the two transverse planes is shown in Fig.7: in the horizontal plane one can clearly see the combined effect of beam energy spread and dispersion in the steps occurring at the dipole positions. In the vertical plane the curve is almost flat after an initial growth. Overall the emittance increase can be contained within 20% and 10% in the horizontal and vertical planes respectively when tracking a newly generated uniform beam (and 22% and 19% when running an end-to-end simulation).
Results are slightly worse when using a 3D point-to-point space charge calculation method instead of the default 2D rings of charge approximation. A different behaviour in the emittance evolution can be observed between the two transverse planes (the horizontal plane being worse and the vertical slightly better in the 3D case), probably due to asymmetries in the beam envelopes that affect the numerical precision of the calculations (see Fig 11 for the beam aspect ratio evolution).

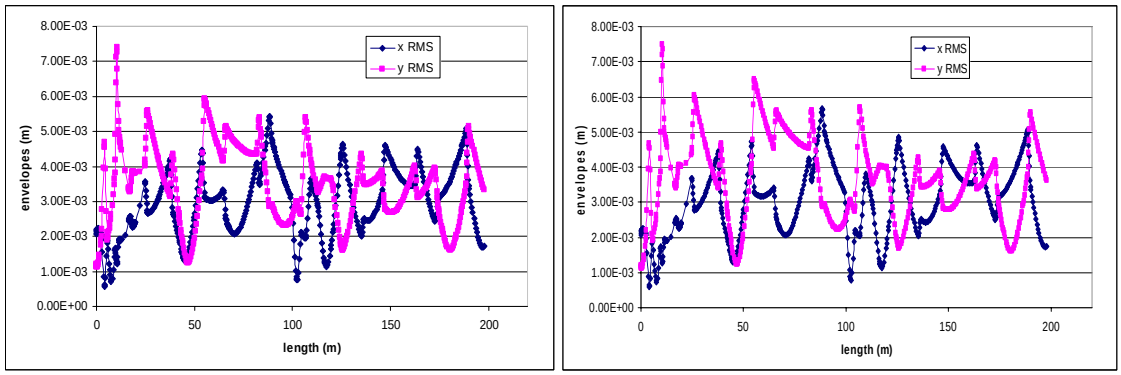

Figure 6 Transverse RMS beam envelopes (initial uniform distribution left, and end to end beam distribution to the right).

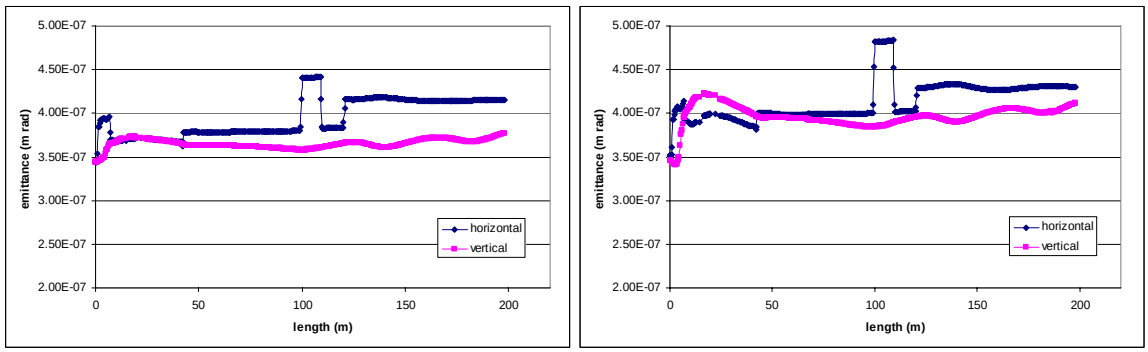

Figure 7 Transverse RMS emittance (left: generated beam, right: end to end beam distribution).

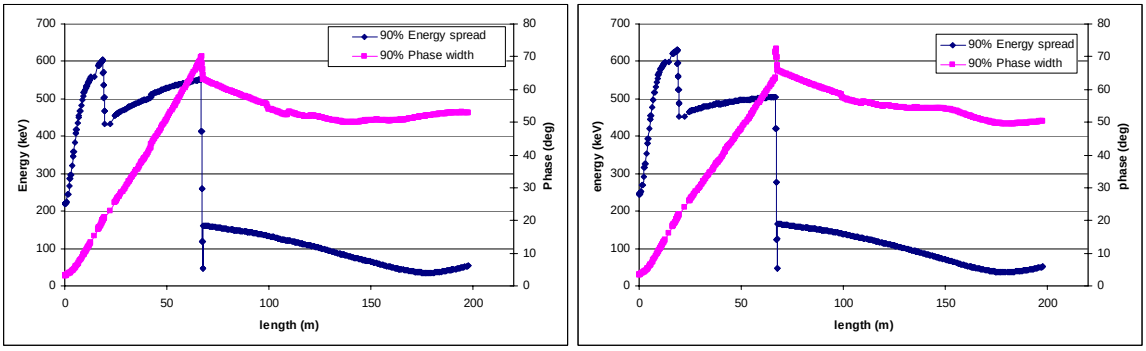

Figure 8 Bunch 90% longitudinal energy spread and phase width (left: uniform beam, right: end-to-end beam distribution).

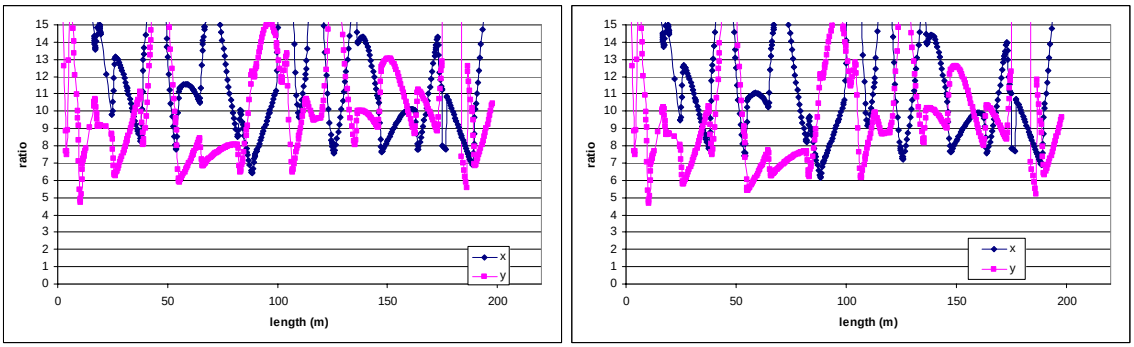

Figure 9 Aperture radius to RMS beam size ratio (left: uniform distribution, right: end-to-end distribution).

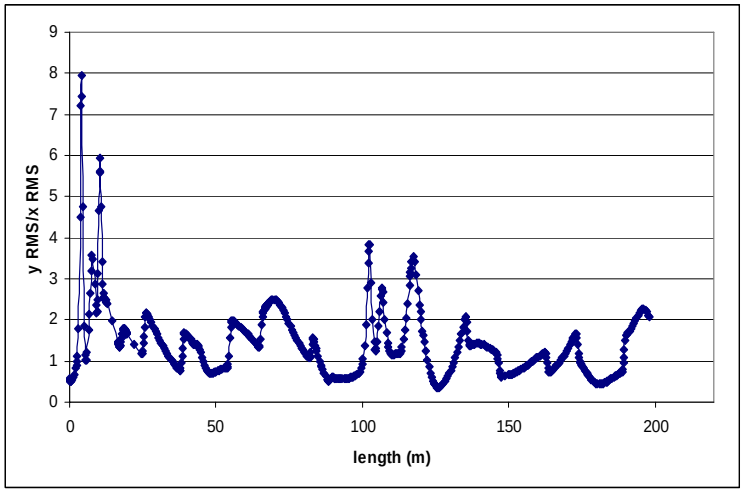

Figure 10 Beam aspect ratio.

In the longitudinal plane, Fig. 8 shows the very rapid increase in energy spread at the beginning of the line, which is then controlled and finally reduced to within 100 keV (for 90% emittance) by tuning of the two debuncher cavities.

The aperture radius to RMS beam size ratio (see Fig. 9) has been kept above a lower limit of 5 even in the line's aperture bottlenecks, which are located at the distributor and septum used for injection in the Booster (a 35mm aperture radius is generally assumed everywhere else).

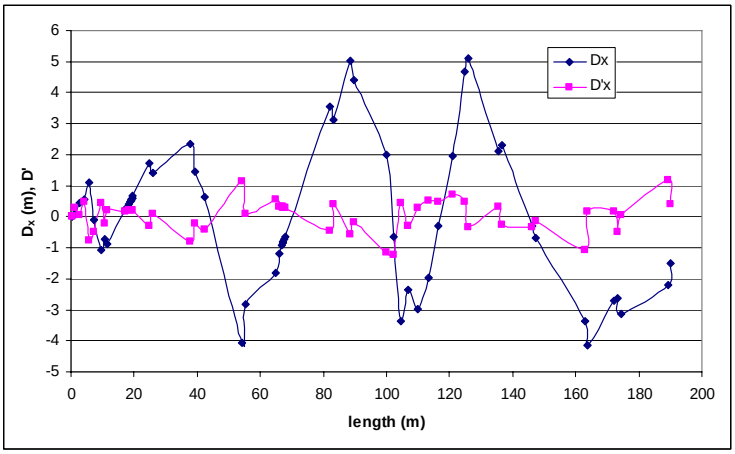

Figure 11 Horizontal dispersion function (and its derivative) of the beam centroid for a uniformly generated beam (I=0 mA).

Fig.11 finally shows the behaviour of the horizontal dispersion function and its derivative along the line for the zero current case (beam centroid dispersion) and uniformly generated input beam distribution. The dispersion is generally larger than in the achromat solution and reaches maximum values of about 5m, but it can be constrained within the required 1.4m maximum limit for injection in the Booster [10].
Final beam parameters for the two cases of an initial uniform beam distribution and end-to-end simulations are summarised in Table 4.

	Uniform				End to end			
	α	β	ε_{out}	$\varepsilon_{out}/\varepsilon_{in}$	α	β	ε_{out}	$\varepsilon_{out}/\varepsilon_{in}$
x	-0.158	4.34 m/rad	0.415 mm mrad	20.6%	-0.192	4.41 m/rad	0.430 mm mrad	22.2%
y	0.996	18.2 m/rad	0.377 mm mrad	9.6%	1.10	19.7 m/rad	0.412 mm mrad	18.7%
z	0.55	1.11 deg/keV	0.532 deg MeV	181.5%	0.46	1.07 deg/keV	0.559 deg MeV	195.8%
x RMS	1.71 mm				1.76 mm			
y RMS	3.35 mm				3.63 mm			
Energy spread	54.4 keV(90% emittance)				51.7 keV (90% emittance)			

Table 4 Final beam parameters for an initial uniform beam distribution and an end-to-end simulation.

Tuning of the line

As mentioned earlier, the most challenging part of the beam dynamics studies has proved to be controlling the beam behaviour at the beginning of the line, owing to a complex interplay of the space charge forces and non-zero dispersion on a beam characterized by a large energy spread and very small phase width.

The two debuncher cavities have been tuned to reduce the energy spread of the beam 1) before entering successive bendings and 2) at the very end of the line to match the acceptance requirements of the Booster. With the solution here presented, the RMS emittance growth of the beam along the total length of the line can be contained within 15-20% in both transverse planes for 2D space charge calculations, compared to a 30-40% increase for the solution with an initial achromat (Fig.4). Results are slightly worse when trying to match for a final α_z~0, and further investigations are currently foreseen to check whether some significant improvement can be achieved by the introduction of a third debuncher cavity in the BI section of the line (after the BHZ30 dipole).

Previous studies on the current Linac2 transfer line [11] and operational experience indicate that having small dispersion at the end of the line can help reduce emittance growth and therefore improve the injection

efficiency of the beam in the Booster. The studies here described for the Linac4 transfer line (but also some more recent results for Linac2 [12]) have in fact demonstrated that trying to limit dispersion or locally matching to zero dispersion along the line can actually induce larger emittance growths on a bunch to bunch basis, whereas allowing for larger values of dispersion but with a more careful tuning of the transverse focusing and beam debunching, one can achieve better results.

However, the situation gets more complicated when considering the pulse emittance, as seen by the PS Booster over injection: in this case in fact the introduction of longitudinal RF errors (jitter) from one bunch to the next in presence of dispersive elements causes some emittance growth in the transverse plane (the x-z coupling converting energy errors into position errors). Studies have been carried out on the effects of an initial beam energy and phase jitter of 271 keV and 1.8 deg RMS respectively, as has been estimated from end-to-end tracking through the linac [13]. This being a dynamic type of error (i.e. varying from bunch to bunch along a pulse), no corrections can be applied by steering the beam back onto its original trajectory, but rather the relative shift between the bunch distributions in phase space will amount to an increase in the effective emittance of a pulse as seen by the Booster. The estimates given above are however somewhat on the conservative side, because they neglect a compensating effect introduced by the debuncher cavities in reducing the initial energy jitter along the line. This has been calculated analytically (and compared with zero current simulation results) to be $\Delta E = V \sin(\Delta\varphi)$, where V is the voltage applied to the cavity and $\Delta\varphi = 2\pi f L / c(1/\beta_{E_j} - 1/\beta_{E_0})$, where f is the frequency, L the distance in between cavities, β_{E0} (β_{Ej}) the relativistic beta at the nominal particle energy or at the energy modified by jitter. The error study has therefore been repeated to account for the concurrence of effects in the longitudinal and transverse planes (basically updating the RF errors after the passage of the beam through each cavity) and the new estimates for the beam shift in the horizontal phase space are Δx=1.1 mm, $\Delta x'$=0.19 mrad for the 1-RMS case and Δx= 3.6 mm $\Delta x'$= 0.57 mrad for the 3-RMS case. This is equivalent to an increase in the pulse horizontal effective emittance (RMS unnormalised) from 0.68 mm mrad to 0.88 mm mrad and 2.39 mm mrad respectively for the 1-RMS and 3-RMS jitter cases.

The energy acceptance of the line has also been estimated by studying how transmission drops as a function of the energy error applied to the input beam distribution (see Fig 12).

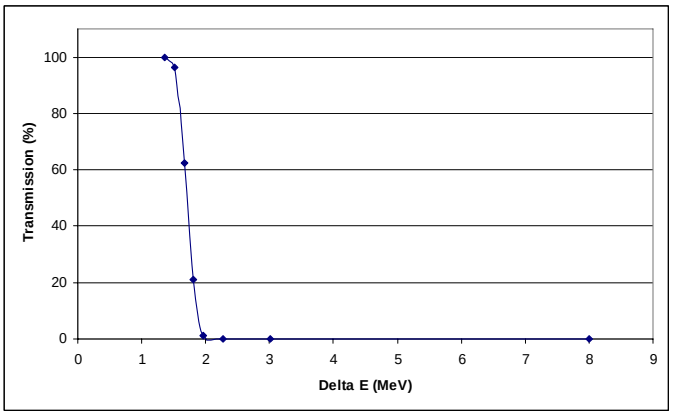

Figure 12 Degradation of the line transmission as a function of initial energy errors.

The maximum tolerance of the line has been calculated to be below a 1% variation in the nominal beam energy (ΔE=1.5 MeV, corresponding to a 96% transmission).

In conclusion, the studies here reported have demonstrated how the beam dynamics for this particular layout of the Linac4 transfer line is fairly complicated and dominated by a strong coupling between the transverse and longitudinal planes as a result of the concurrence of space charge, dispersion and energy jitter effects. As a consequence, trying to optimise for one parameter at a time usually has detrimental effects on some other quantity (minimization of the energy spread at the PSB injection vs transverse emittance increase, minimization of the dispersion along the line - and therefore of the pulse emittance growth- vs the single bunch emittance growth etc..). The layout here described represents a good trade-off and balance between all these parameters.

Appendix A

Element	Field (T/m)	Element	Field (T/m)
Quadrupole 1	-4.64	Quadrupole 13	-2.90
Quadrupole 2	6.56	Quadrupole 14	2.76
Quadrupole 3	-8.36	Quadrupole 15	-1.86
Quadrupole 4	-6.49	Quadrupole 16	1.50
Quadrupole 5	6.93	Quadrupole 17	-1.60
Quadrupole 6	-3.53	Quadrupole 18	2.06
Quadrupole 7	-1.68	Quadrupole 19	-1.46
Quadrupole 8	1.15	Quadrupole 20	0.67
Quadrupole 9	-2.34	Quadrupole 21	1.11
Quadrupole 10	2.23	Quadrupole 22	-3.90
Quadrupole 11	-2.86	Quadrupole 23	2.41
Quadrupole 12	2.92		

Table 5 Settings of the quadrupoles in the part of the transfer line to be newly built.

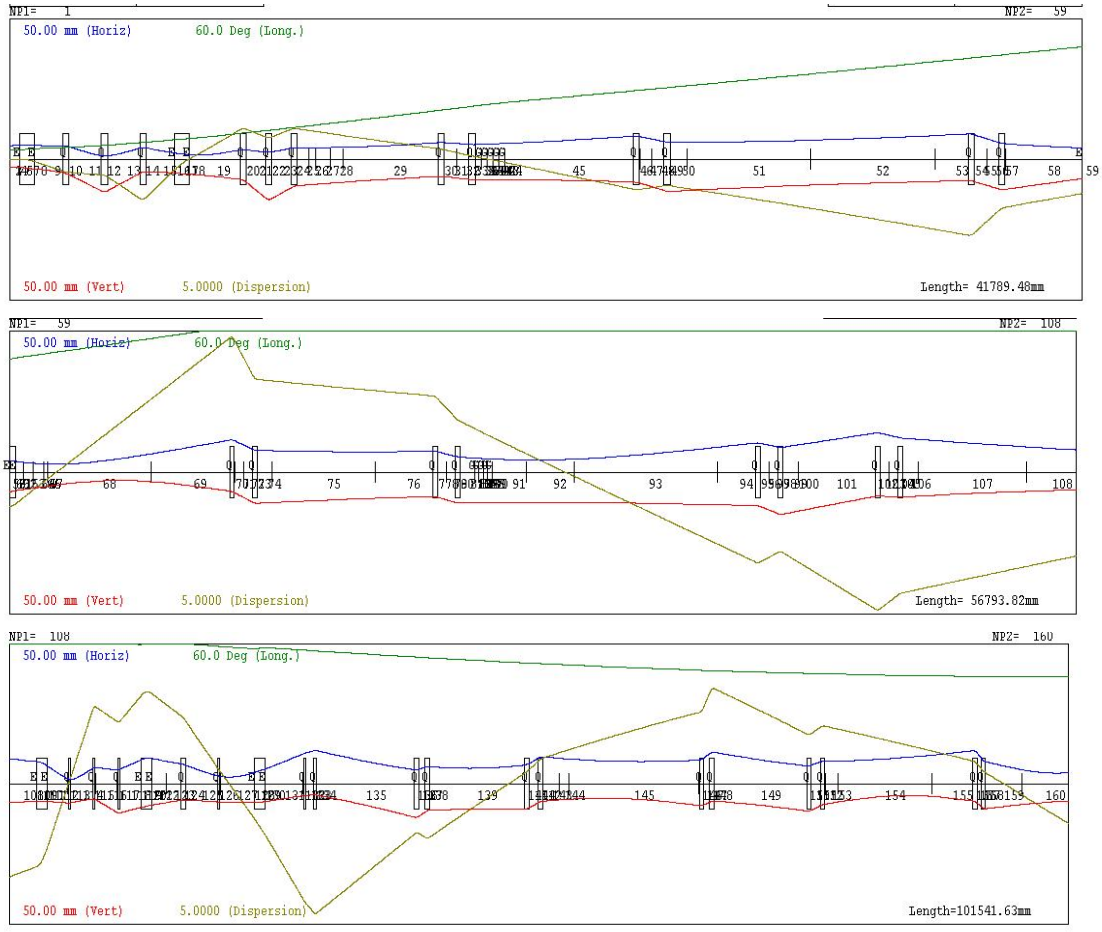

Figure 10 Sketch of the transfer line showing magnet positions, beam envelopes (blue and red lines), longitudinal phase spread (green) and dispersion (ochre). For better clarity the line has been split into 3 consecutive segments (top to bottom), but not on the same scale.

Appendix B

At the time of studying the integration of the present scheme for the Linac4 transfer line in the complex of existing accelerator structures, a few problems and incompatibilities were highlighted that have prompted a slight revision of the layout here described in the so-called "inflector zone" area. In particular the bendings of the last two dipoles in the sketch shown in Fig.1 have been changed from +31/+31 degrees to +41.5/+20.5 degrees, with a consequent redefinition of the magnet families specified in Table 1 to allow for an increased length of approximately 1300 mm for the type B bends (at an unchanged B=1.0125 T) and a 4-1 grouping of the dipoles in family type A and B respectively.

A re-tuning of the line was carried out and the final settings of all elements are listed in Table 6, in sequential order from the exit point of Linac4.

Element	**s (m)**	**Magnetic length (mm)**	**Gradient (T/m)**	**Angle (deg)**	**Voltage (MV)**
Dipole1	0.7	573		17.275	
Quad1	2.2	250	-4.64		
Quad2	3.7	250	6.56		
Quad3	5.2	250	-8.36		
Dipole2	6.7	573		17.275	
Quad4	9.1	250	-6.49		
Quad5	10.1	250	6.93		
Quad6	11.09	250	-3.53		
Quad7	16.83	250	-1.68		
Quad8	18.02	250	1.15		
Debuncher1	18.85	1150			0.51
Quad9	24.43	250	-2.34		
Quad10	25.63	250	2.23		
Quad11	37.47	250	-2.86		
Quad12	38.67	250	2.92		
Dipole3	41.96	350		-10.55	
Quad13	53.66	250	-2.90		
Quad14	54.86	250	2.76		
Quad15	64.45	250	-1.86		
Quad16	65.65	250	1.50		
Debuncher2	67.03	1150			0.675
Quad17	81.65	250	-1.60		
Quad18	82.85	250	2.06		
Quad19	88.03	250	-1.46		
Quad20	89.23	250	0.67		
Dipole4	100.43	1380		41.5	
Quad21	103.64	250	1.11		
Quad22	106.3	250	-3.90		
Quad23	108.95	250	2.41		
Dipole5	111.82	680		20.5	
LT.QFW70	112.92	467	0.42		
LT.QDN75	116.30	255	-2.82		
LT.BHZ30	120.23	1006		22	
LTB.QFN10	124.54	255	3.26		
LTB.QDN20	125.54	255	-3.36		

LTB.QFW30	135.29	461	1.23		
LTB.QDW40	136.29	461	-0.94		
LTB.QFW50	145.84	461	1.10		
LTB.QDW60	147.14	461	-1.17		
BI.Q10	162.58	462	1.48		
BI.Q20	163.58	462	-1.55		
BI.Q30	172.90	462	0.72		
BI.Q40	174.20	462	-0.73		
BI.Q50	188.84	466	-2.0		
BI.Q60	189.59	466	2.0		

Table 6 Final specifications of the transfer line elements: from left to right column, the longitudinal coordinate of the centre (m), the magnetic length (mm), quadrupole gradients (T/m), dipole bending angles (deg) and the debuncher voltages (MV).

Simulation results for an end-to-end initial beam distribution (obtained from tracking the beam from the RFQ input to the end of the SCL) and 2D space charge approximation method are shown in Figs 11-13.

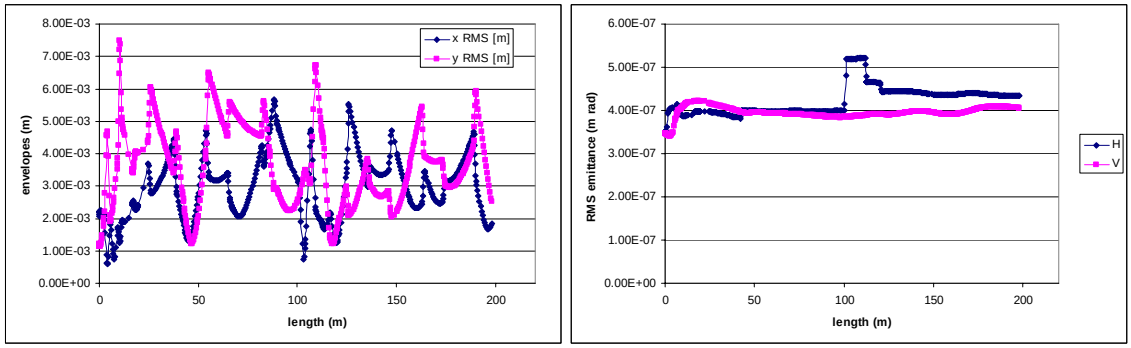

Figure 11 Transverse RMS beam envelopes (left) and emittances (right).

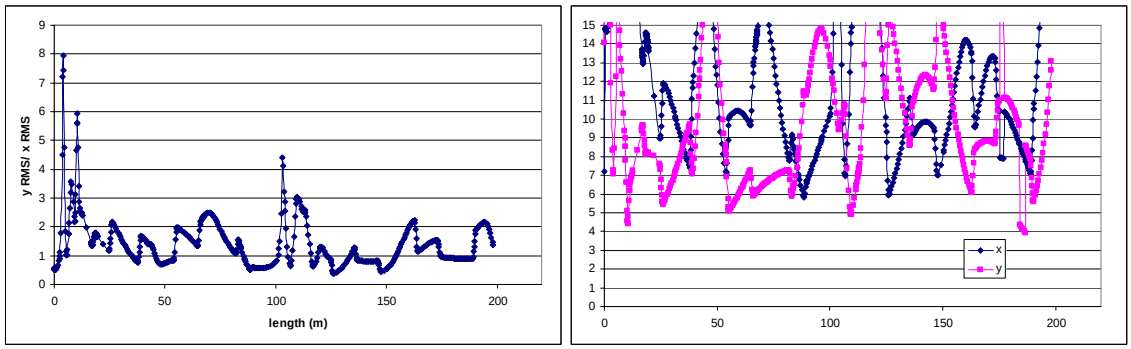

Figure 12 Beam aspect ratio (left) and aperture radius to RMS beam size ratio (right).

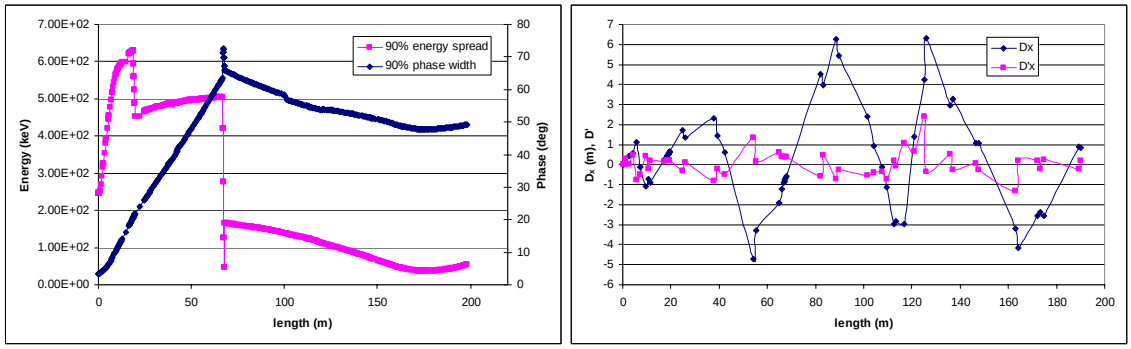

Figure 13 90% longitudinal energy spread and phase width (left) and horizontal dispersion functions (right, for I=0mA, uniform initial beam distribution and debuncher cavities turned off).

RMS beam sizes are again mostly contained within 5-6 mm and the aperture radius to RMS beam size ratio has been mostly kept above a lower limit of 5, apart from at a couple of bottlenecks in the vertical plane located at the initial bend in the line and further on in the injection septum (a 33mm physical aperture radius is generally assumed unless otherwise specified, with a beampipe radius of 35mm). The RMS transverse emittance increase is approximately 23% and 17% in the horizontal and vertical planes respectively. In the longitudinal phase space (Fig 13 left), the initial large energy spread is reduced to around 55 keV at the end of the line for a 90% emittance value. Finally the horizontal dispersion function (Fig 13 right for a zero current case, initial uniform beam distribution and debuncher cavities switched off) has a maximum absolute value of just over 6m and can be reduced to approximately 1m to satisfy the injection constraints in the PS Booster.
Table 7 summarises the final beam parameters at Booster injection for an end-to-end simulation.

	End to end			
	α	β	ε_{out} RMS	$\varepsilon_{out}/\varepsilon_{in}$ (RMS)
x	-0.473	4.80 m/rad	0.434 mm mrad	23.3%
y	1.390	9.66 m/rad	0.405 mm mrad	16.7%
z	0.576	1.04 deg/keV	0.561 deg MeV	196.8%
x RMS	1.84 mm			
y RMS	2.52 mm			
Energy spread	54.5 keV (90% emittance)			
D_x (D'_x) @inj.	0.85 m (0.2)			

Table 7 Final beam parameters for an end-to-end simulation.

References

[1] "Conceptual design of the SPL II", CERN-2006-006 (2006).
[2] "Linac4 Technical Design Report", CERN-AB-2006-084 (2006).
[3] M.Eshraqi, A.Lombardi,"Alternative options for the Linac4 Transfer Line", CERN-AB-Note-2006-044 (2006).
[4] T.Zickler, private communication.
[5] M.Pasini, private communication.
[6] M.Binjonaid, F. Gerigk, internal note (2006).
[7] R. Thomas, "H- stripping in the Booster proton injection line", AD Booster Technical Note 79, BNL (1987).
[8] M.Martini, C.R.Prior, "High-intensity and high-density charge-exchange injection studies into the CERN PS Booster at intermediate energies", EPAC 2004 Proceedings, (2004).
[9] B.Goddard, private communication.

[10] K.Hanke, private communication.
[11] K.Hanke, “An achromatic optics for the Linac2 to Booster transfer line”, AB-Note-2006-001 OP (2006).
[12] S.Lanzone, A.Lombardi, “Path simulations of the Linac2 transfer line”, AB-Note-2006-045 (2006).
[13] M.Baylac, “Error studies of Linac4”, presentation at ICFA-HB2006 workshop.